FINITE DIFFERENCE COMPUTATION OF AIRFOILS WITH BLUNT NOSES IN TRANSONIC FLOWS

Wang Die Qian (D. Q. Wang)
Northwestern Polytechnical University,
Xi"an, China

ICAS-82-6.3.1

Abstract

This paper presents a finite difference computation for transonic steady potential flow around an airfoil. In transonic flow changes along the direction of the flow are larger than those transverse to it, and the perturbation velocity component in the direction normal to airfoil chord is assumed to be much smaller than the undisturbed flow velocity; thus the simplified velocity potential equation in ref. (9) is used in the present paper. But its premise and derivation are improved in rigorousness here. The schemes of finite difference proposed by Murman-Cole are used by the author. The exact boundary condition on the surface is applied at the chord of airfoil and fitted into the velocity potential difference equations. The finite difference equations for the velocity potential are solved by the line-relaxation method. The convergence can be significantly improved by chord-wise(x-axis) line relaxation along the line from leading edge to far field and y-wise line relaxation for the remainder of the field. The method described in the present paper overcomes some of the difficulties encountered in small-perturbation theory and improves the accuracy of pressure distribution, especially at the nose of the airfoil. In general, this algorithm is not more costly than that of small-perturbation theory in terms of storage requirements and computer time. Numerical examples are included and the results agree fairly well with those in references (3), (6) and (7).

1. Introduction

The finite difference method for solving small-perturbation equation was proposed by Murman-Cole(1). Because of assumption of small-perturbation, the pressure distributions, especially at the leading edge and in the neighbourhood of it are not good enough. The absolute value of the pressure coefficient on the upper surface obtained by small-perturbation theory is too small, especially the small-perturbation theory does not reflect adequately the rapid expansion around the nose. So in some papers, for instance refs. (4) & (5), the pressure distribution obtained by small-perturbation computation is corrected empirically. In these papers, the absolute value of x-direction disturbed velocity obtained by small-perturbation computation is multiplied by $M_\infty^{-q}/M_\infty^{-p}$ (in (4)&(5), $M_\infty < 1$, two indices p, q were chosen to obtain the best agreement with certain exact solutions), and consequently the absolute value of pressure coefficient is increased. Ref. (5) showed by numerical experimentation that a refined mesh could adequately handle leading edge singularity . But numerical experimentation may not always be available. The difficulties of small-perturbation computation arise from the singularity at the leading edge. The difficulties may be avoided by ensuring that the mesh or grid points of the numerical calculation do not lie on the leading edge, or even on points where the slopes of the airfoil surface are large. This may lead to the computation of an unrealistic shape and it is possible that some results obtained by a certain grid are satisfactory, while some others are not.

But small-perturbation finite difference computation has the merit of being quite economical in computer time. Ref. (9) presented a more satisfactory simplified perturbation potential equation but its premise and derivation are improved in rigorousness in the present paper. In applying the above mentioned equation to the numerical solution of flow problems, ref. (2) proposes that the boundary condition at every point on the airfoil surface can be fitted into the equation and in this way some of the difficulties encountered in small perturbation theory are overcome. But the resulting improvement does not require substantial increase in computer time. In order to accelerate convergence, different line relaxation algorithms are used at different places of the flow field.

2. The Perturbation Velocity Potential Equation

In the transonic case, the lateral extent of the field is large and the changes along the direction of free stream flow are of main importance. Typical flow fields in transonic case are illustrated in the following figures.

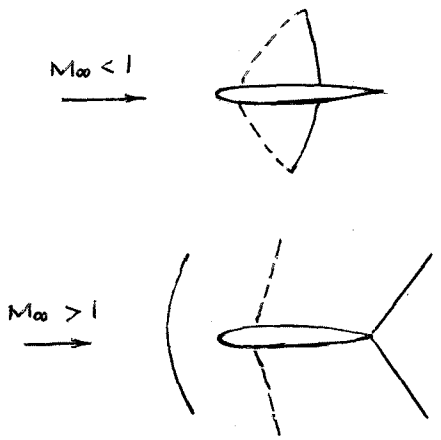

At the leading edge and in the neighbourhood of it the order of magnitude of the perturbation velocity component in the chord direction may be as large as U_∞, i.e. $|\varphi_x/U_\infty| \doteq 1$. So we assume that

1) low angle of attack i.e. $\alpha \ll 1$,

2) the perturbation velocity component in the direction normal to the airfoil chord is much smaller than the undisturbed flow velocity i.e. $|v/U_\infty| \ll 1$, while the perturbation velocity component in the chord wise direction u may not be so,

3) $|\partial u/\partial x| \gg |\partial u/\partial y|$; $|\partial v/\partial y| \sim |\partial u/\partial y|$.

The equation of motion for steady frictionless flow is

$$(1-\frac{u_1^2}{a^2})\frac{\partial u_1}{\partial x}+(1-\frac{u_2^2}{a^2})\frac{\partial u_2}{\partial y}+(1-\frac{u_3^2}{a^2})\frac{\partial u_3}{\partial z}-$$
$$-\frac{u_1u_2}{a^2}(\frac{\partial u_1}{\partial y}+\frac{\partial u_2}{\partial x})-\frac{u_2u_3}{a^2}(\frac{\partial u_2}{\partial z}+\frac{\partial u_3}{\partial y})-$$
$$-\frac{u_1u_3}{a^2}(\frac{\partial u_3}{\partial x}+\frac{\partial u_1}{\partial z})=0 \qquad (1)$$

here u_1, u_2, u_3 are the velocity components in x, y, z directions respectively, a is the local sound speed. If the x-axis lies along the chord, then

$u_1 = U_\infty\cos\alpha + u = U_\infty\cos\alpha + \varphi_x$

$u_2 = U_\infty\sin\alpha + v = U_\infty\sin\alpha + \varphi_y$

$u_3 = w = \varphi_z$

here u, v, w are perturbation velocities, and φ is the disturbed velocity potential. a^2 may be obtained in terms of the perturbation velocities from the energy equation . Substituting in Eq. (1), dividing by a_∞^2 , we obtain

$$(1-M_\infty^2\cos^2\alpha)\frac{\partial u}{\partial x}+\frac{\partial v}{\partial y}+\frac{\partial w}{\partial z}$$
$$= M_\infty^2\left[(\gamma+1)\frac{u\cos\alpha}{U_\infty}+\frac{\gamma+1}{2}\frac{u^2}{U_\infty^2}+\frac{\gamma-1}{2}\frac{v^2+w^2}{U_\infty^2}+\right.$$
$$\left.+(\gamma-1)\frac{v}{U_\infty}\sin\alpha\right]\frac{\partial u}{\partial x}+M_\infty^2\left[(\gamma-1)\frac{u\cos\alpha}{U_\infty}+\right.$$
$$\left.+\frac{\gamma+1}{2}\frac{v^2}{U_\infty^2}+\frac{\gamma-1}{2}\frac{w^2+u^2}{U_\infty^2}+\sin^2\alpha+(\gamma+1)\frac{v}{U_\infty}\sin\alpha\right]\frac{\partial v}{\partial y}+$$
$$+M_\infty^2\left[(\gamma-1)\frac{u\cos\alpha}{U_\infty}+\frac{\gamma+1}{2}\frac{w^2}{U_\infty^2}+\frac{\gamma-1}{2}\frac{u^2+v^2}{U_\infty^2}+\right.$$
$$\left.+(\gamma-1)\frac{v}{U_\infty}\sin\alpha\right]\frac{\partial w}{\partial z}+M_\infty^2\left[(\cos\alpha\sin\alpha+\frac{v}{U_\infty}\sin\alpha+\right.$$
$$\left.+\frac{v}{U_\infty}\cos\alpha+\frac{v}{U_\infty}\frac{u}{U_\infty})(\frac{\partial u}{\partial y}+\frac{\partial v}{\partial x})+\frac{w}{U_\infty}(\cos\alpha+\frac{u}{U_\infty})(\frac{\partial u}{\partial z}+\right.$$
$$\left.+\frac{\partial w}{\partial x})+\frac{w}{U_\infty}(\sin\alpha+\frac{v}{U_\infty})(\frac{\partial w}{\partial y}+\frac{\partial v}{\partial z})\right] \qquad (2)$$

where γ is the ratio of specific heats. For two-dimensional flow, under the above assumptions, Eq. (2) becomes

$$\frac{1-M_\infty^2[1+(\gamma+1)u/U_\infty+\frac{\gamma+1}{2}u^2/U_\infty^2]}{1-M_\infty^2[(\gamma-1)u/U_\infty+\frac{\gamma-1}{2}u^2/U_\infty^2]}\frac{\partial u}{\partial x}+\frac{\partial v}{\partial y}$$
$$=\frac{M_\infty^2[(\alpha+v/U_\infty)(1+u/U_\infty)]}{1-M_\infty^2[(\gamma-1)u/U_\infty+\frac{\gamma-1}{2}u^2/U_\infty^2]}(\frac{\partial u}{\partial y}+\frac{\partial v}{\partial x}) \qquad (3)$$

in which terms of second and higher order in the coefficients of the derivatives of the perturbation velocities have been neglected. Note that under the condition of weak shock the flow may be considered irrotational, and that at the leading edge or in the neighbourhood of it $u \sim -U_\infty$, $|u| < U_\infty$ and everywhere else $|u/U_\infty| \ll 1$. So the righthand side of Eq. (3) can be neglected as compared with the lefthand side. Thus Eq. (3) becomes

$$(1-M^2)\varphi_{xx}+\varphi_{yy}=0 \qquad (4)$$

where
$$M^2=\frac{1+2\xi}{1-(\gamma-1)\xi M_\infty^2}M_\infty^2 \qquad (5)$$

and
$$\xi=(1+\frac{1}{2}\frac{\varphi_x}{U_\infty})\frac{\varphi_x}{U_\infty}$$

From Eq. (4) we can see that as $|\varphi_x/U| \ll 1$ and $M_\infty \sim 1$, $M^2 \doteq M_\infty^2+(\gamma+1)\varphi_x M_\infty^2/U_\infty$, Eq. (4) becomes the small-perturbation equation. On the other hand, as $\varphi_x \doteq -U_\infty$ (at the leading edge and in the neighbourhood of it), $\xi=-1/2$ and $M^2=0$, Eq. (4) becomes Laplace equation. So Eq. (4) is superior to the small-perturbation equation. The superiority of Eq. (4) lies in that:

The description of the flow field by Eq. (4) is superior compared with that by small-perturbation equation. At the blunt leading edge Eq. (4) approximates to Laplace equation. There the boundary condition is compatible with Eq. (4), but not with the small-perturbation equation. So the main difficulty of small-perturbation equation is overcome by Eq. (4). However, same as for small-perturbation equation, the axes of characteristic cones are parallel to x-axis, and the mixed schemes of finite difference are used along x-direction only, so its algorithm is not more costly than small-perturbation equation in terms of storage requirements and computer time.

3. The Boundary Condition on the Surface

The surface boundary condition at any point is compatible with the potential equation . In this paper the exact boundary condition on the surface is applied on the chord of airfoil and fitted into the velocity potential difference equations.

The boundary condition can be written as,

$$(\varphi_x+U_\infty\cos\alpha)\cos(n,x)+(\varphi_y+U_\infty\sin\alpha)\cos(n,y)=0,$$

where n denotes the outward direction normal to the surface. If $\cos(n,y)\neq 0$, then

$$\varphi_y(x,\pm 0)=U_\infty\cos\alpha(\frac{dy_{u,l}}{dx}-\tan\alpha)+\varphi_x(x,\pm 0)\frac{dy_{u,l}}{dx} \qquad (6)$$

If $\cos(n,y)=0$, then

$$\varphi_x(x,0)=-U_\infty\cos\alpha \qquad (7)$$

But the linearized small-perturbation boundary condition is

$$\varphi_y(x,\pm 0)=U_\infty(\frac{dy_{u,l}}{dx}-\alpha)$$

i.e. the φ_y is directly proportional to $dy_{u,l}/dx$. Thus in the neighbourhood of leading edge, an unrealistic supersonic zone may exist. So the mesh or grid points of numerical calculation must not lie on the leading edge and the points where the slopes of airfoil surface are too large in the small-perturbation computation. But by Eq. (4) and boundary condition (6) and (7) these difficulties have been overcome.

4. The Kutta Condition

The Kutta condition indicates the smooth flow past the sharp trailing edge. It is approximately satisfied by the following equations:

$$\varphi_y(X>X_T, +0) = \varphi_y(X>X_T, -0) \qquad (8)$$

$$\varphi(X>X_T, +0) - \varphi(X>X_T, -0) = \varphi(X_T, +0) - \varphi(X_T, -0) \qquad (9)$$

where x_T denotes the x-coordinate of the trailing edge.

The y-line relaxation is used behind the airfoil. We fit Eq. (8), (9) into the velocity potential difference equations as follows: at y=+0, y=0, y=-0 three y-direction mesh points ju, ja and jl are arranged (see figure below),

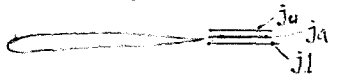

at ja, φ_y is unknown and at ju, jl, φ is unknown.

5. The Boundary Condition for the Far-field

According to the analysis of ref. (8), for $M_\infty<1$, only that part of the potential which is associated with lift will be used for the far-field representation for lifting wings, since the other terms are of higher order and may be neglected. Thus we have

$$\varphi = -\frac{\Gamma}{2\pi}\left[\operatorname{arctg}\frac{my}{x} + \begin{cases} -\pi \ (\text{I quadrant}) \\ \pi \ (\text{IV quadrant}) \\ 0 \ (\text{II, III quadrant}) \end{cases}\right]$$

For $M_\infty>1$, the disturbed potential for far-field may be written as follows

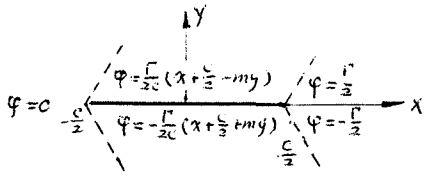

where $\Gamma = \varphi_{i_T,ju} - \varphi_{i_T,jl}$

$m = \sqrt{|1-M_\infty^2|}$

i_T denotes the x-direction station of the mesh point at the trailing edge.

6. The Schemes of Finite Difference and Relaxation Algorithm

The mixed schemes of finite difference are used along x-direction only. When M<1, central schemes are used

$$\varphi_x = \frac{\varphi_{i+1,j}\Delta x_{i-1}^2 + \varphi_{i,j}(\Delta x_i^2 - \Delta x_{i-1}^2) - \varphi_{i-1,j}\Delta x_i^2}{\Delta x_{i-1}\Delta x_i(\Delta x_{i-1}+\Delta x_i)} + O(\Delta x^2),$$

$$\varphi_{xx} = 2\,\frac{\varphi_{i+1,j}\Delta x_{i-1} - \varphi_{i,j}(\Delta x_{i-1}+\Delta x_i) + \varphi_{i-1,j}\Delta x_i}{\Delta x_{i-1}\Delta x_i(\Delta x_{i-1}+\Delta x_i)} + O(\Delta x),$$

When M≥1, side schemes are used

$$\varphi_x = \frac{\varphi_{i,j}[(\Delta x_{i-2}+\Delta x_{i-1})^2 - \Delta x_{i-1}^2] - \varphi_{i-1,j}(\Delta x_{i-2}+\Delta x_{i-1})^2 + \varphi_{i-2,j}\Delta x_{i-1}^2}{\Delta x_{i-2}\Delta x_{i-1}(\Delta x_{i-2}+\Delta x_{i-1})} + O(\Delta x^2), \qquad (10)$$

$$\varphi_{xx} = 2\,\frac{\varphi_{i,j}\Delta x_{i-2} - \varphi_{i-1,j}(\Delta x_{i-2}+\Delta x_{i-1}) + \varphi_{i-2,j}\Delta x_{i-1}}{\Delta x_{i-2}\Delta x_{i-1}(\Delta x_{i-2}+\Delta x_{i-1})} + O(\Delta x), \qquad (11)$$

where i, j denot the stations of the mesh points in x and y-directions respectively.

The central schemes are used for the partial derivatives along y-direction, whatever M may be.

The boundary condition on the surface is fitted into the difference equations of the perturbation velocity potential as follows

$$(\varphi_{yy})_{i,ju} = \frac{2}{\Delta y_{ju}}\left[\frac{\varphi_{i,ju+1} - \varphi_{i,ju}}{\Delta y_{ju}} - (\varphi_y)_{i,ju}\right],$$

and $(\varphi_{yy})_{i,jl} = \frac{2}{\Delta y_{jl-1}}\left[(\varphi_y)_{i,jl} - \frac{\varphi_{i,jl} - \varphi_{i,jl-1}}{\Delta y_{jl-1}}\right]$,

where φ_y is computed according to Eq. (6). At cos(n,y)=0 Eq. (7) is fitted into the difference equations of the perturbation velocity potential in the following way: $\varphi_{i-2,j}$ is solved from Eq. (10) and Eq. (7), to get $\varphi_{i-2,j} = f(\varphi_{i,j}, \varphi_{i-1,j})$, then substituted in Eq. (11).

On the airfoil surface (mainly at the leading edge and in the neighbourhood of it), in order to ensure the truncation error to be of the first order accuracy of step size when substituting differences for partial derivatives in Eq. (4), scheme of second order accuracy of step size for φ_x must be used.

Along the chord-wise line from blunt nose to far field, the salient feature of flow due to perturbation is the deceleration of the flow velocity. In order to accelerate convergence x-line relaxation algorithm is used along the line from leading edge to far field and the y-line relaxation is used for the remainder of the field. For wing section NACA 0012, angle of attack $\alpha = 2°$, $M_\infty = 0.63$, 17×13 meshes and $|\Delta\varphi|_{max} = |\varphi_{i,j}^{(n)} - \varphi_{i,j}^{(n-1)}|_{max} = 10^{-6}$ (n denotes the iterative run, and both the chord and U_∞ are assumed to be unity), by using the method described in the present paper, the time of convergence is reduced to about 10% of the time required when y-line relaxation algorithm is used all over the field. As for the other airfoils computed in this paper $|\Delta\varphi|_{max}$ is reduced to the order of magnitude 0.5×10^{-3} after iterative runs of 30~50. It can be seen that the convergence is accelerated effectively by the method described in the present paper.

7. Numerical Examples

In the numerical examples in this paper, both the undisturbed velocity and the chord are assumed to be unity. The exact Bernoulli formula is used in calculating pressure coefficients on the surface

$$C_p = \frac{2}{\gamma M_\infty^2}\left\{\left[1 - \frac{(\gamma-1)M_\infty^2}{2}\left(\frac{\varphi_x\cos\alpha}{U_\infty} + \frac{\varphi_x^2}{2U_\infty^2} + \frac{\varphi_y\sin\alpha}{U_\infty} + \frac{\varphi_y^2}{2U_\infty^2}\right)\right]^{\frac{\gamma}{\gamma-1}} - 1\right\},$$

where the partial derivatives are calculated by the central schemes.

Some airfoils in ref. (3) and (7) were calculated. The result of calculation of airfoil with shock on it was compared with experimental results in ref. (6).

The calculations show that denser meshes result in better accuracy (see Fig. 3).

The results of numerical examples are shown in Figs. 1-7. It can be seen that the accuracy of the method described in the present paper is fairly satisfactory.

8. Concluding Remarks

An improved method of finite difference

computation based on a simplified potential equation is described in the present paper. Small-perturbation equation does not give a good fit at blunt nose of the airfoil, but equation (4) does. The potential equation and surface boundary condition described in the present paper overcome some of the difficulties encountered in small-perturbation theory and improve the accuracy of pressure distribution calculations. Thus the method described in the present paper is in the author's opinion superior to small-perturbation theory; moreover, the algorithm of the method described in the present paper is not more costly than that of the method of small-perturbation theory in terms of storage requirements and computer time. But at the leading edge or in the neighbourhood of it, at even not very large angle of attack, the y-direction perturbation velocity component may not be small as compared with U_∞. It is the weakness still existing when using Eq. (4).
In order to accelerate convergence, x-line relaxation is used along the line from leading edge to far field, and y-line relaxation is used for the remainder of the field. In this way the convergence is effectively accelerated.

The numerical examples indicate that the accuracy of the method described in the present paper is fairly satisfactory and denser meshes result in better accuracy .

Acknowledgement

The author wishes to thank Professor S. J. Luo for making extremely valuable suggestions.

References

1. Murman, E. M. and Cole, J. D., Calculation of Plane Steady Transonic Flows, AIAA J, Vol. 9, 1971, pp. 114-121.
2. Wang, Die Qian (D. Q. Wang), Finite Difference Calculation of Airfoils with Blunt Noses,The Aeronautical Science Conference of Northwestern Polytechnical University, 1977, Xi'an, China.
3. Lock, R. C., Test Cases for Nnmerical Methods in Two-Dimensional Transonic Flows, AGARD Report No. 575, 1970.
4. Langley, M. J., Numerical Methods for Two-Dimensional and Axisymmetric Transonic Flows, A.R.C. C.P. No. 1376, 1977.
5. Murman, E.M. and Krupp, J.A., The Numerical Calculation of Steady Transonic Flows past Thin Lifting Aerofoils and Slender Bodies, AIAA J., Vol. 10., 1972, pp. 880-886.
6. Steger, J. L. and Lomax, H., Transonic Flow about Two Dimensional Airfoils by Relaxation Procedures, AIAA J., Vol. 10, 1972, pp. 49-54.
7. Gentry, Arvel E. and Oliver, Wayne R., Investigation of Aerodynamic Analysis Problems in Transonic Maneuvering, Vol. 1, AD-737293, 1971.
8. Klunker, E. B., Contribution to Methods for Calculating the Flow about Thin Lifting Wings at Transonic Speeds-Analytic Expressions for the Far Field, NASA TND-6530, 1971.
9. Pan, Nai Qiang (N. Q. Pan), Wang, Wie Fu (W.F. Wang) and Xu, Shon Jiang (S. J .Xu), Finite Difference Computation of Wing-Body Combination, Beijing Research Institute, China Precision Machinery Corp., 1977 (unpublished).

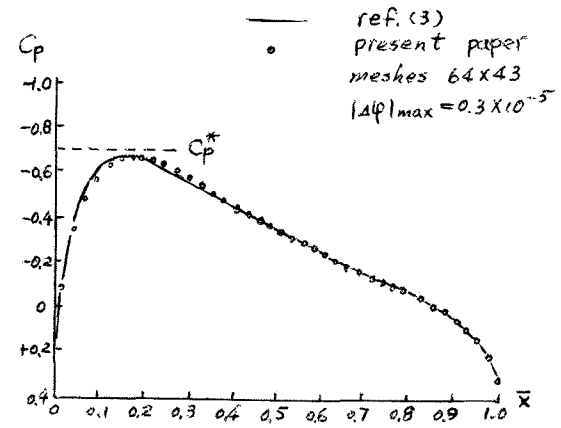

Fig. 1. NACA 0012, $M_\infty = 0.72$, $\alpha = 0°$

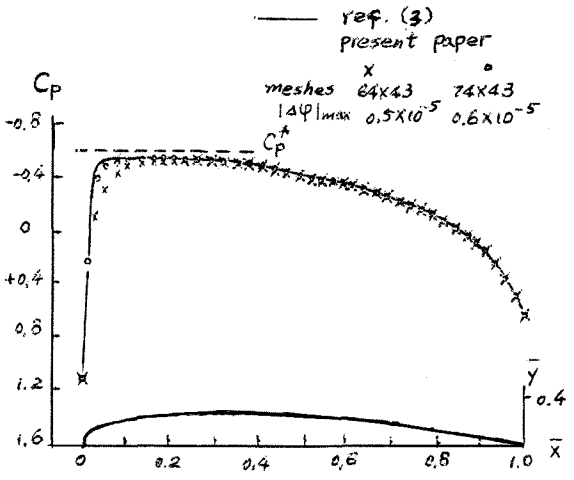

Fig. 2. NLR 0.10-0.75-1.25, $M_\infty = 0.7454$, $\alpha = 0°$

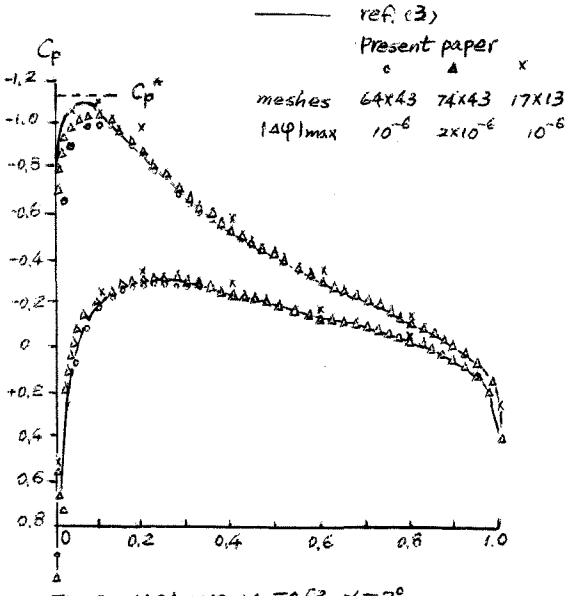

Fig. 3. NACA 0012, $M_\infty = 0.63$, $\alpha = 2°$

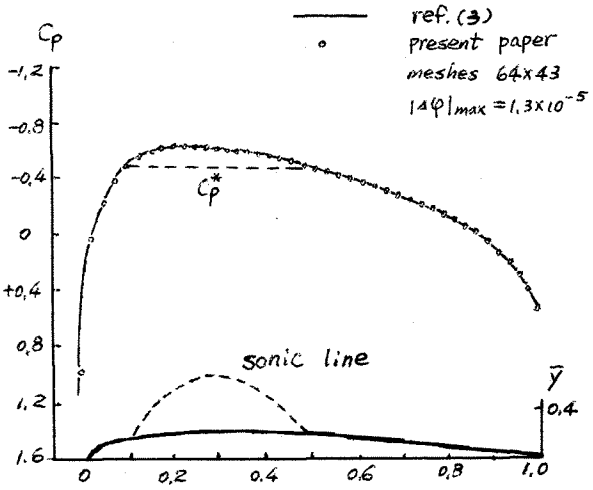

Fig. 4. NLR 0.1100-0.75-0.9, $t/c = 0.1138$, $M_\infty = 0.7$[illegible], $\alpha = 0°$

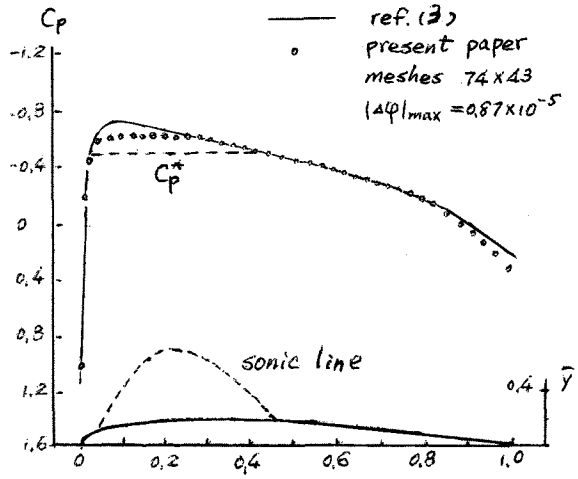

Fig. 5. NLR 0.11-0.75-1.25, $t/c = 0.1163$, $M_\infty = 0.7861$, $\alpha = 0°$

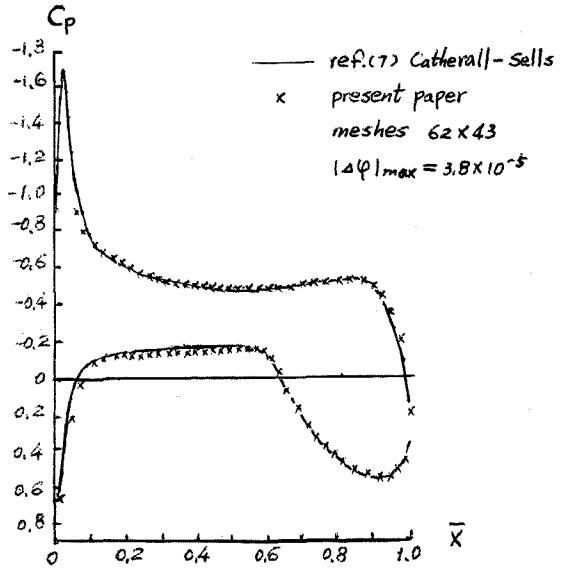

Fig. 6. DSMA 523 aft roaded airfoil, $M_\infty = 0.5$, $\alpha = 0°$

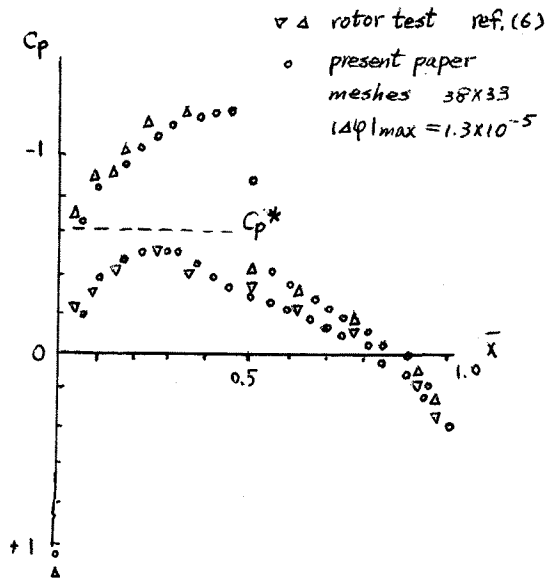

Fig. 7. NACA 0012, $M_\infty = 0.75$, $\alpha = 2°$